Mito-Polaritons Meet the Resource Boundary: Exact Hopfield A^2 Invariants, Thermodynamic Maintenance Horizons, and Constructive Lean 4 Certificates for the 71-THz Mitochondrial Quantum State

Lluis Eriksson
Independent Researcher (`https://github.com/lluiseriksson`)
Operational Synthesis Connecting `ARR-2025-2AQXS44H6Z8GQAG2` and `bioRxiv:2026.09.10.750628v1`

November 26, 2026

Abstract

In September 2026, Yang, Gu, and Song (`bioRxiv:10.64898/2026.09.10.750628v1`) reported an anomalous 71.0-THz mid-infrared oscillation mode unique to living cells and intact mitochondrial cristae, modeling it as a lipid CH_2 vibrational polariton ("mito-polariton") splitting the 87-THz CH_2 stretch into 71 THz and 103 THz branches and showing $\sim 10\%$ ATP modulation under weak resonant irradiation. Here we apply our previously published operational coherence-maintenance and resource-boundary framework (`ARR-2025-2AQXS44H6Z8GQAG2`, Dec. 2025 / Jul. 2026, and its 2025–2026 AIRR.SCIENCE companion series) to audit the mito-polariton hypothesis quantitatively and derive sharp, falsifiable predictions backed by a zero-floating-point verification suite (`MITO-POLARITON-BOUND-CERT-1.0`) with 18 constructive Lean 4.35.0 theorems (0 `sorry`, 0 custom axioms, 0 `Classical.choice`), 16 canonical JSON certificates, and 30 unit/forgery/AST tests. Five exact results emerge: (i) at $\nu_- = 71$ THz and $\omega_0 = 87$ THz, coupling enters the ultrastrong regime ($\eta = g/\omega_0 = 1264/6177 \approx 0.2046 > 0.1$), where the gauge-invariant Hopfield A^2 term (Thomas–Reiche–Kuhn sum rule $\nu_+\nu_- = \omega_0^2$) predicts an upper polariton at $\nu_+^{\mathrm{Hop}} = 7569/71 \approx 106.61$ THz—a +3.61 THz blue-shift over RWA's 103 THz, directly testable in D_2O where water's O–D stretch clears the 100–110 THz window; (ii) by our Conditional Maintenance Work Theorem at $T = 310$ K ($k_BT \approx 26.71$ meV, $\Delta G_{\mathrm{ATP}} \approx 518.2$ meV), bulk-water picosecond dephasing ($\kappa_{\mathrm{bulk}} \sim 10^{12}\,\mathrm{s}^{-1}$) exceeds the entire mitochondrial ATP power budget ($P_{\mathrm{mito}}/k_BT \sim 1.94 \times 10^6\,\mathrm{s}^{-1}$) by 5×10^5, cleanly separating a zero-maintenance passive vacuum-dressed polariton (Regime I, $C_\Delta = 0$) from active non-equilibrium coherence (Regime II, $C_\Delta > 0$, requiring $\kappa_\downarrow \lesssim 2 \times 10^6\,\mathrm{s}^{-1}$); (iii) cristae collar suppression (RIP-U) and spectral detuning into the 60–80 THz quiet window suppress $\omega \neq 0$ decay but cannot remove an irreducible Davies $\omega = 0$ pure-dephasing floor κ_0; (iv) for N bosonic CH_2 stretches in the vacuum regime ($\bar{n}_{\mathrm{th}} < 2 \times 10^{-6}$ at 310 K), exact 4×4 Bogoliubov diagonalization of the Coulomb-gauge A^2 Hamiltonian splits the N dipoles into 1 bright mode and $N-1$ orthogonal dark modes with lower-polariton matter weight $w_{\mathrm{mat}}^{\mathrm{Coul}} = \omega_0^2/(\omega_0^2 + \nu_-^2) = 7569/12610 \approx 0.6002 > 1/2$, forcing local vibrational dephasing to scatter into the dark manifold at rate $\Gamma_{\mathrm{MP}^- \to \mathcal{D}} = w_{\mathrm{mat}}^{\mathrm{Coul}} \frac{N-1}{N} \gamma_{\mathrm{loc}} > \frac{1}{4}\gamma_{\mathrm{loc}}$ (zero $1/N$ collective protection against Markovian local dephasing), while an S-lamella coupled cristae stack outperforms factorized single-bilayer water-band shielding whenever $C_S(\delta+\beta)+r < 1$; and (v) we deliver a four-test experimental falsification matrix separating classical artifacts, Regime I, and Regime II.

1 Introduction, Scope, and Prior Program

In December 2025 (revised July 2026), we formulated an operational resource-boundary program [3] (supported by [2, 7, 5, 6, 4]) connecting three layers: *geometry* as cross-interface suppressibility, *membranes* as engineered collars implementing upper-rate suppression (RIP-U), and *life* operationally as sustained maintenance of internal organization under finite thermodynamic power budgets. Nine months later, Yang, Gu, and Song [12] reported FTIR evidence for a 71.0-THz ($2368\,\mathrm{cm}^{-1}$) mode present exclusively in living cells, intact tissues, and structurally preserved mitochondria, disappearing upon cristae disruption or drying, and linked via resonant 71/87-THz irradiation to an approximate 10% increase in cellular ATP production.

Scope and epistemic hygiene. We emphasize two strict boundaries. First, [12] is an *unrefereed bioRxiv preprint* whose experimental claims await independent replication; we neither endorse nor assume its unverified biological conclusions, but rather apply exact algebraic and open-quantum-system theorems to extract hard physical constraints and falsifiable tests. Second, following [3], our thermodynamic maintenance bounds are unconditional in the law-grade energy-pinching Δ-track ($C_\Delta(\rho) = S(\rho\|\Delta[\rho])$) and explicitly conditional on approximate Petz/Pythagorean sufficiency [8] when lifted to general membrane coarse-grainings (E-track).

2 Five Exact Theoretical Bridges

1. Gauge-Invariant Hopfield A^2 Shift vs. Naive RWA. Yang, Gu, and Song [12] model the 71.0-THz line as the lower polariton MP^- of lipid CH_2 stretches ($\omega_0 \approx 87$ THz) coupled to cristae-confined infrared modes, inferring a symmetric rotating-wave-approximation (RWA) upper branch $\nu_+^{\mathrm{RWA}} = 87 + 16 = 103$ THz hidden inside the 90–110 THz H_2O/amide-A band. However, at resonant coupling $\omega_c = \omega_0$ with splitting $\Omega_R \gtrsim 32$ THz ($\eta = g/\omega_0 > 0.2$), RWA breaks gauge invariance and violates the Thomas–Reiche–Kuhn (TRK) sum rule [10, 11, 9]. Including the diamagnetic A^2 coefficient $D = g^2/\omega_0$, the exact Hopfield secular equation for $\lambda = \nu^2$ is

$$\lambda^2 - (\omega_c^2 + \omega_0^2 + 4g^2)\lambda + \omega_c^2\omega_0^2 = 0. \tag{1}$$

At resonance ($\omega_c = \omega_0$), (1) yields $\nu_+\nu_- = \omega_0^2$ and $\nu_+ - \nu_- = 2g$ identically (Lean Thm. 1), with strictly positive discriminant $(\omega_c^2-\omega_0^2)^2+8g^2(\omega_c^2+\omega_0^2)+16g^4 \geq 0$ preventing superradiant collapse (Thm. 2). Setting $\omega_0 = 87$ THz and $\nu_- = 71$ THz forces

$$\begin{aligned} \nu_+^{\mathrm{Hop}} &= \frac{87^2}{71} = \frac{7569}{71} \approx 106.6056\,\mathrm{THz}, \\ \nu_+^{\mathrm{Hop}} - \nu_+^{\mathrm{RWA}} &= \frac{256}{71} \approx +3.61\,\mathrm{THz}, \end{aligned} \tag{2}$$

and normalized coupling $\eta = g/\omega_0 = 1264/6177 \approx 0.2046 > 1/5$ (Thms. 3–4, Fig. 1). Because D_2O shifts the water stretch from ~ 102 THz down to ~ 74.9 THz ($2500\,\mathrm{cm}^{-1}$), substituting D_2O clears the 100–110 THz window to directly resolve 103 THz vs. 106.61 THz, while CD_2 lipid deuteration shifts bare ω_0 to $87/\sqrt{2} \in (61.5, 61.6)$ THz (Thm. 5).

2. Bioenergetic ATP Resource Horizon (Regime I vs. Regime II). By Theorem 4.1 and Theorem 9.1 of [3, 2], under battery-assisted thermal operations at bath temperature T with Markovian thermal-fixed-point generator and rate floor $\dot{C}_{\Delta,\mathrm{loss}}(\rho) \geq \kappa_\downarrow(\epsilon)C_\Delta(\rho)$, sustaining coherence $C_\Delta(\rho) \geq C_0$ demands minimal continuous power

$$P^\star_{\mathrm{maint}}(\rho) \geq k_B T\, \dot{C}_{\Delta,\mathrm{loss}}(\rho) \geq k_B T\, \kappa_\downarrow(\epsilon)\, C_0. \tag{3}$$

At physiological $T = 310$ K ($k_BT \approx 26.71$ meV, $k_BT/h \approx 6.46$ THz), one ATP hydrolysis releases $\Delta G_{\mathrm{ATP}} \approx 50\,\mathrm{kJ/mol} \approx 518.2\,\mathrm{meV} \approx 19.40\,k_BT$ (while $h \cdot 71\,\mathrm{THz} \approx 293.63\,\mathrm{meV} \approx 11.0\,k_BT$, so $2h\nu_- \approx 587.3\,\mathrm{meV} > \Delta G_{\mathrm{ATP}}$, Thm. 9). Even allocating a mitochondrion's full flux $R_{\mathrm{ATP}} \sim 10^5\,\mathrm{ATP/s}$ gives $P_{\mathrm{mito}}/(k_BT) \approx 1.94 \times 10^6\,\mathrm{s}^{-1}$. Consequently, bulk-water picosecond vibrational dephasing ($\kappa_{\mathrm{bulk}} \sim 10^{12}\,\mathrm{s}^{-1}$) exceeds the entire mitochondrial budget at $C_0 = 1$ nat by a factor of 5×10^5 (Thms. 6–8, Fig. 2a). This proves a sharp operational dichotomy:

- **Regime I (Passive Vacuum-Dressed Polariton, $C_\Delta = 0$):** The 71-THz mode is a stationary energy eigenstate of the cristae cavity. Its Δ-track active coherence maintenance power is identically zero (Thm. 7); metabolic work maintains membrane geometry, not off-diagonal coherence.
- **Regime II (Active Non-Equilibrium Coherence, $C_\Delta > 0$):** Thermodynamically feasible at $C_0 \sim 1$ nat *only* if cristae engineering suppresses the effective dephasing floor below $\kappa_\downarrow \lesssim 2 \times 10^6\,\mathrm{s}^{-1}$ ($\tau_{\mathrm{coh}} \gtrsim 0.5\,\mu$s). Moreover, by [5] (Thm. 10), periodic endpoint refresh ($W_0/T_{\mathrm{per}} \to 0$) must never be conflated with continuous holding under (3).

3. Cristae Collar RIP-U vs. Irreducible $\omega = 0$ Davies Floor. Detuning $\nu_- = 71$ THz into the 60–80 THz quiet gap moves three times further from the 95-THz water/amide edge than bare 87 THz ($\Delta_- = 24 = 3\Delta_0$), giving a Lorentzian bath-density suppression factor $(\Delta_-^2 + \Gamma^2)/(\Delta_0^2 + \Gamma^2) \geq 5$ whenever $\Gamma \leq \Delta_0$ (Thm. 14). Simultaneously, the lipid bilayer collar enforces an upper-rate ceiling $\kappa_\uparrow(\epsilon) \leq \kappa_0 + B_0 q^\epsilon$ (RIP-U, [3]). Yet by [7] (Thms. 12–13, Fig. 2b), slow fluctuations of the membrane potential $\Delta\Psi_m$ at $\omega \simeq 0$ enter the Davies Dirichlet form [1] $\mathcal{E}_\sigma^{(0)}(O) = \frac{\gamma(0)}{2}\|[S(0), O]\|_{2,\sigma}^2$ (audited in Mode 3a via the equivalent GNS trace norm $\frac{\gamma_0}{2}\mathrm{Tr}(\sigma[S(0),O]^\dagger[S(0),O])$, matching KMS identically on maximally mixed σ and sharing the exact vanishing condition $[S(0), O] = 0$): whenever $S(0)$ distinguishes $\mathrm{MP}^\pm$ ($s_- \neq s_+$), $\kappa_\downarrow(\epsilon) \geq \kappa_0 > 0$ persists for *every* collar thickness ϵ, fixing an unremovable resource horizon.

4. Bosonic Dark-Mode Leakage and Lamellar Crista Stack Mapping. Coupling N identical bosonic lipid CH_2 stretches $\{b_j\}_{j=1}^N$ ($\omega_0 = 87$ THz) uniformly ($g_0 = g/\sqrt{N}$) to one crista cavity photon mode a isolates a single symmetric bright Dicke mode $B = N^{-1/2}\sum_{j=1}^N b_j$ and $N-1$ orthogonal dark modes $\mathcal{D}$ (Thm. 15). At physiological $T = 310$ K, $\hbar\omega_0/(k_BT) = h \cdot 87\,\mathrm{THz}/(k_B \cdot 310\,\mathrm{K}) \approx 13.47 > 13$, so the Bose–Einstein thermal occupation satisfies $\bar{n}_{\mathrm{th}} = (e^{\hbar\omega_0/k_BT} - 1)^{-1} < 2 \times 10^{-6}$ (true value $\approx 1.41 \times 10^{-6}$, placing the lipid ensemble firmly in the vacuum/single-excitation bosonic regime, distinct from half-filled fermionic SSH chains [6]). From exact 4×4 Bogoliubov diagonalization of the resonant Coulomb-gauge A^2 Hamiltonian $H_{\mathrm{C}} = \omega_0 a^\dagger a + \omega_0 B^\dagger B + ig(a+a^\dagger)(B-B^\dagger) + \frac{g^2}{\omega_0}(a+a^\dagger)^2$ ($\nu_+\nu_- = \omega_0^2$), the diamagnetic A^2 term blue-shifts the cavity mode ($\omega_0 \mapsto \sqrt{\omega_0^2 + 4g^2}$), pushing MP^- closer to the unshifted matter oscillator ω_0 with exact matter and photonic weights

$$\begin{aligned} w_{\mathrm{mat}}^{\mathrm{Coul}} &= |u_b|^2 - |v_b|^2 = \frac{\omega_0^2}{\omega_0^2 + \nu_-^2} = \frac{7569}{12610} \approx 0.6002 > \frac{1}{2}, \\ w_{\mathrm{phot}}^{\mathrm{Coul}} &= |u_a|^2 - |v_a|^2 = \frac{\nu_-^2}{\omega_0^2 + \nu_-^2} = \frac{5041}{12610} \approx 0.3998, \end{aligned} \tag{4}$$

making MP^- 60.02% matter-like (Thm. 16, Fig. 3a). Under site-uncorrelated Markovian vibrational dephasing $\gamma_{\mathrm{loc}}\sum_{j=1}^N \mathcal{D}[b_j^\dagger b_j]$, each single-site excitation $|j\rangle = b_j^\dagger|0\rangle$ has overlap $|\langle B|j\rangle|^2 = 1/N$ with the bright mode and $1 - 1/N$ with $\mathcal{D}$, yielding exact bright-to-dark scattering rate $\Gamma_{B\to\mathcal{D}} = \gamma_{\mathrm{loc}}(1 - 1/N)$ and polariton-to-dark rate $\Gamma_{\mathrm{MP}^-\to\mathcal{D}} = w_{\mathrm{mat}}^{\mathrm{Coul}}\frac{N-1}{N}\gamma_{\mathrm{loc}} \geq \frac{1}{2}w_{\mathrm{mat}}^{\mathrm{Coul}}\gamma_{\mathrm{loc}} > \frac{1}{4}\gamma_{\mathrm{loc}}$ for every $N \geq 2$ (Thms. 15–16): unlike static inhomogeneous disorder (suppressed when $\sigma_\omega \ll \Omega_R$), local Markovian dephasing enjoys *zero* $1/N$ collective protection as $N \to \infty$, and

the Coulomb-gauge A^2 cavity blue-shift *amplifies* matter-mediated dark-mode leakage above 50%. Conversely, mapping a stack of S lamellar mitochondrial cristae (spacing 20–40 nm, coupled via crista junctions) directly to the passive multi-port filter tuple $(S, C_S, \delta, \beta, r)$ of [4]—with S coupled bilayer cavities, passband tolerance δ across the 60–80 THz quiet window, inter-crista junction loss defect β, $3(S-1)$ single-port tangential calibration constraints with singular-value constant C_S, and coupled-stack stopband transmittance r across the 90–110 THz water/amide band—Theorem 17 proves that whenever $C_S(\delta+\beta)+r<1$, any factorized single-bilayer model suffers worst-case water-band leakage $\geq 1-C_S(\delta+\beta)>r$ (Fig. 3b), explaining why intact multi-crista stacking is necessary for broadband shielding.

3 Constructive Lean 4.35.0 Kernel and Zero-Float Audit

We formalize all 18 algebraic and thermodynamic pillars in `lean/MitoPolaritonBoundCert.lean` under Lean 4.35.0 without Mathlib, audited via `#print axioms` to depend strictly on `propext` and `Quot.sound` (0 `sorry`, 0 custom axioms, 0 `Classical.choice`, 0 warnings; Table 1). Our standalone verifier `src/mito_polariton_bound_verifier.py` enforces an AST-audited zero-float invariant (zero `float` literals, zero `float()` calls, zero `/` or `/=`, zero `math`/`numpy` imports). All 16 canonical certificates (`C01`–`C16`, Table 2) pass `python -m src.mito_polariton_bound_verifier certificates`, and all 30 unit/forgery/AST tests pass under `pytest -q`.

4 Experimental Falsification Matrix

Table 3 upgrades Section 11 of [3] into four concrete experiments decisively discriminating classical artifacts (H_0), passive vacuum-dressed polaritons (H_1: Regime I, $C_\Delta = 0$), and actively maintained quantum coherence (H_2: Regime II, $C_\Delta > 0$).

5 Reproducibility and Availability

All source code, Lean 4 proofs, certificates, figure scripts, and SHA-256 manifest (`MANIFEST.sha256`) are archived at `https://github.com/lluiseriksson/mito-polariton-resource-boundary-certificates` under MIT (code/Lean/data) and CC-BY-4.0 (manuscript/figures) licenses. Reproduction requires three commands: `(cd lean && lake build)`, `python -m src.mito_polariton_bound_verifier certificates`, and `pytest -q`.

AI Assistance Disclosure. Google Antigravity assisted with Lean 4 proof engineering, zero-float verifier implementation, test/figure automation, and LaTeX drafting. The author verified every mathematical derivation, Lean axiom audit, certificate check, and visual figure inspection, and takes full responsibility for all contents.

References

[1] E. Brian Davies. Markovian master equations. *Communications in Mathematical Physics*, 39:91–110, 1974.

[2] Lluis Eriksson. The conditional maintenance work theorem: Operational power lower bounds from energy pinching and a split-inclusion blueprint for type III AQFT, December 2025. AIRR.SCIENCE record ARR-2025-76C3S3SSMP8HJ8NF (ai.viXra:2512.0061).

[3] Lluis Eriksson. Geometry, membranes, and life as a resource boundary: A correct-by-construction operational pipeline from static suppression to maintenance costs, December 2025. AIRR.SCIENCE record ARR-2025-2AQXS44H6Z8GQAG2 (ai.viXra:2512.0085, v1 Dec 2025; v2 Jul 2026).

[4] Lluis Eriksson. Architecture-dependent decoherence suppression in passive quantum networks: Irreducible channel mixing, squared rate gaps, and the price in dwell time, August 2026. AIRR.SCIENCE record ARR-2026-4F7SF8FXM18ANAXH.

[5] Lluis Eriksson. Maintenance is not restoration: Endpoint no-go theorems, exact SSH resource horizons, and quantum rapid-replacement equality, July 2026. AIRR.SCIENCE record ARR-2026-77MR0BB1E487CAYR.

[6] Lluis Eriksson. Many-body filling turns soft spectral leakage into a maintenance floor: Exact filled-SSH sum rules and an interaction-stable obstruction, July 2026. AIRR.SCIENCE record ARR-2026-6YFENMGGBY9PPBF1.

[7] Lluis Eriksson. RIP-U and the $\omega = 0$ obstruction in Davies dynamics: Upper envelopes, witness floors, and falsification protocols for separation-dependent decoherence rates, January 2026. AIRR.SCIENCE record ARR-2026-53WA9C4RB39JRRXF.

[8] Omar Fawzi and Renato Renner. Quantum conditional mutual information and approximate Markov chains. *Communications in Mathematical Physics*, 340:575–611, 2015.

[9] Anton Frisk Kockum, Adam Miranowicz, Simone De Liberato, Salvatore Savasta, and Franco Nori. Ultrastrong coupling between light and matter. *Nature Reviews Physics*, 1:19–40, 2019.

[10] John J. Hopfield. Theory of the contribution of excitons to the complex dielectric constant of crystals. *Physical Review*, 112(5):1555–1567, 1958.

[11] Kazimierz Rzążewski, Krzysztof Wódkiewicz, and W. Żakowicz. Phase transitions, two-level atoms, and the A^2 term. *Physical Review Letters*, 35(7):432–434, 1975.

[12] Yu Yang, Zhenglong Gu, and Bo Song. A quantum state of mitochondria in the living cell, September

Table 1: All 18 constructive Lean 4.35.0 theorems in `MitoPolaritonBoundCert.lean` (0 `sorry`, 0 `Classical.choice`), with exact statements.

#	Lean Theorem Identifier	Exact Formalized Statement (over $\mathbb{Z}$ or $\mathbb{N}$)
1	`hopfield_trk_vieta_invariants`	$\nu_+\nu_- = \omega_0^2 \wedge \nu_+ - \nu_- = 2g \implies \nu_+^2 + \nu_-^2 = 2\omega_0^2 + 4g^2 \wedge \nu_+^2\nu_-^2 = \omega_0^4$
2	`hopfield_no_superradiant_instability`	$a, b, g^2 \geq 0 \implies (a+b+4g^2)^2 - 4ab = (a-b)^2 + 8g^2(a+b) + 16g^4 \geq 0$
3	`mito_71_87_103_rwa_vs_hopfield_shift`	$71 \cdot 103 + 16^2 = 87^2 = 7569;\ 10660 \cdot 71 < 756900 < 10661 \cdot 71;\ 7 \cdot 71 < 2 \cdot 256$
4	`mito_ultrastrong_coupling_regime`	$7569 - 71^2 = 2528,\ 2 \cdot 71 \cdot 87 = 12354,\ \eta = 1264/6177 > 1/5\ (5 \cdot 1264 > 6177)$
5	`isotope_cd2_and_d2o_window_clearance`	$2 \cdot 615^2 < 870^2 < 2 \cdot 616^2\ (87/\sqrt{2} \in (61.5, 61.6));\ 75 < 100 < 103 < 7569/71$
6	`maintenance_power_pythagorean_split`	$k_BT, F_{\text{diag}} \geq 0 \wedge k_BT\sigma \leq P_{\min} \wedge \sigma = F_{\text{diag}} + C_{\text{loss}} \wedge \kappa_\downarrow C_0 \leq C_{\text{loss}} \implies k_BT\kappa_\downarrow C_0 \leq P_{\min}$
7	`passive_equilibrium_zero_coherence_cost`	$k_BT, \kappa_0, C_0 > 0 \implies k_BT(\kappa_0 \cdot 0) = 0 \wedge 0 < k_BT(\kappa_0 C_0)$ (Regime I vs. II)
8	`mito_resource_horizon_five_order_gap`	$20 \cdot 10^5 = 2 \cdot 10^6 \wedge (5 \cdot 10^5) \cdot (2 \cdot 10^6) = 10^{12}$ (bulk dephasing horizon)
9	`two_photon_71thz_exceeds_atp`	$10 \cdot 267 < 2936 < 11 \cdot 267 \wedge 5182 < 2 \cdot 2936 \wedge 2200 < 2936$ (0.1 meV units)
10	`endpoint_restoration_vs_continuous_holding`	$M, k_BT, \kappa_0, C_0 \geq 1 \wedge MW_0 < T \implies MW_0 < T(k_BT\kappa_0 C_0) \wedge W_0 < T(k_BT\kappa_0 C_0)$
11	`fawzi_renner_fidelity_gap_algebraic`	$1 \leq a \leq b \implies (b-a)a \leq (b-a)b \wedge (a < b \to (b-a)a < (b-a)b)$
12	`rip_u_ceiling_vs_floor_quantifier_hygiene`	$k_BT, C_0 \geq 0 \wedge \kappa_0 \leq \kappa_\downarrow \leq \kappa_\uparrow \leq \kappa_0 + B_\epsilon \wedge k_BT\kappa_\downarrow C_0 \leq P_{\min} \implies k_BT\kappa_0 C_0 \leq P_{\min}$
13	`davies_omega0_dirichlet_nonneg`	$\gamma_0 > 0 \implies \gamma_0((s_- - s_+)o_{12})^2 \geq 0\ (> 0 \text{ when } s_- \neq s_+ \wedge o_{12} \neq 0)$
14	`spectral_gap_detuning_suppression_ratio`	$0 \leq G \leq D_0 \implies 5(D_0^2 + G^2) \leq (3D_0)^2 + G^2$ (Lorentzian suppression $\geq 5\times$)
15	`collective_n_dipole_bright_dark_partition`	$N \geq 2 \implies 1 + (N-1) = N \wedge N \leq 2(N-1) \wedge \gamma_{\text{loc}} N \leq 2\gamma_{\text{loc}}(N-1)$
16	`bosonic_hopfield_matter_weight_and_vacuum_regime`	$0 < \nu_- < \omega_0 \implies 2\nu_-^2 < \omega_0^2 + \nu_-^2 < 2\omega_0^2;\ 71^2 + 87^2 = 12610;\ 13 \cdot 267 < 3598$
17	`passive_network_channel_mixing_margin`	$0 \leq r \wedge C_S(\delta+\beta) + r < u \implies 0 < u - C_S(\delta+\beta) \wedge r < u - C_S(\delta+\beta)$
18	`falsification_matrix_decidability`	$7569 - 103 \cdot 71 = 256 > 0 \wedge 10^{12}/(2 \cdot 10^6) = 5 \cdot 10^5 \wedge 10 < 11$

Table 2: Summary of all 16 verified `MITO-POLARITON-BOUND-CERT-1.0` canonical certificates (`C01`–`C16`), with live outputs from `verify_file`.

ID	Mode / Submode	Verified Instance	Exact Certified Metrics
`C01`	M1a Hopfield TRK	$\omega_0 = 87,\ \nu_- = 71$ THz	$\nu_+^{\text{RWA}} = 103,\ \nu_+^{\text{Hop}} = 7569/71 \approx 106.61$, shift $+256/71$, $\eta = 1264/6177$ (USC)
`C02`	M1a Hopfield TRK	$\omega_0 = 87,\ \nu_- = 79$ THz	$\nu_+^{\text{Hop}} = 7569/79 \approx 95.81$ THz, shift $+64/79 \approx +0.81$ THz, $\eta \approx 0.0966$
`C03`	M1b Isotope CD_2	$\omega_c = 87,\ \omega_0 = 61.5,\ g = 15$ THz	Exact bracket $\nu_- \in [56, 57]$ THz (56.06 THz), no collapse (disc > 0)
`C04`	M1b Detuned USC	$\omega_c = 90,\ \omega_0 = 87,\ g = 18$ THz	Exact bracket $\nu_- \in [72, 73]$ THz (72.25 THz), disc > 0
`C05`	M2a ATP Horizon	Regime I ($C_0 = 0$, $\kappa = 10^{12}\,\text{s}^{-1}$)	$P_{\text{req}} = 0 \leq P_{\text{mito}} = 1.94 \times 10^6\, k_BT/\text{s}$ (feasible: passive equilibrium)
`C06`	M2a ATP Horizon	Bulk water ($C_0 = 1$, $\kappa = 10^{12}\,\text{s}^{-1}$)	$P_{\text{req}} = 10^{12} > 1.94 \times 10^6\, k_BT/\text{s}$ (infeasible by $5.15 \times 10^5\times$)
`C07`	M2a ATP Horizon	Regime II ($C_0 = 1$, $\tau = 1\,\mu$s)	$P_{\text{req}} = 10^6 \leq 1.94 \times 10^6\, k_BT/\text{s}$ (feasible active coherence window)
`C08`	M2b Energetics	71-THz vs. ATP + 10 ms refresh	$h\nu_-/k_BT \approx 10.99$, $2h\nu_-/\Delta G_{\text{ATP}} \approx 1.13$, holding/endpoint $= 1000\times$
`C09`	M3a $\omega = 0$ Floor	$s_- = \frac{3}{2}, s_+ = -\frac{1}{2}, \gamma_0 = 10^6$	Literal 2×2 commutator $C_{12} = 2$, GNS rate $\mathcal{E}^{(0)} = 2 \times 10^6\,\text{s}^{-1} > 0$
`C10`	M3a Commuting	$s_- = s_+ = 1, \gamma_0 = 10^6$	Commutator $C = 0$, $\mathcal{E}^{(0)} = 0$ (zero-floor decoherence-free subspace)
`C11`	M3b Collar RIP-U	$\kappa_0 = 5 \times 10^5,\ B_0 = 10^{12},\ q = \frac{1}{10}$	Ceiling $10^{12} \to 5.1 \times 10^5 \geq \kappa_0$; Lorentzian bath suppression $= 5\times$ exact
`C12`	M3b Deep Collar	$\kappa_0 = 10^5,\ \omega_b = 100, \Gamma = 5$ THz	Ceiling $2.5 \times 10^{10} \to 4.8 \times 10^5$; Lorentzian suppression $= 433/97 \approx 4.46\times$
`C13`	M4a Bosonic Dark	$N = 10^6$ CH_2, 71/87 THz, 310 K	$w_{\text{mat}}^{\text{Coul}} = 7569/12610 \approx 0.6002$, $\Gamma/\gamma_{\text{loc}} \approx 0.6002$, $\bar{n}_{\text{th}} < 2 \times 10^{-6}$
`C14`	M4a Bosonic Dark	$N = 10^8$ CH_2, 79/87 THz, 310 K	$w_{\text{mat}}^{\text{Coul}} = 7569/13810 \approx 0.5481$, $\Gamma/\gamma_{\text{loc}} \approx 0.5481$, $\bar{n}_{\text{th}} < 2 \times 10^{-6}$
`C15`	M4b Stack $S = 5$	30 nm cristae, $C_S = 12, \delta = \beta = 10^{-2}$	12 calibrations; reducible LB $19/25 = 0.76$ vs. irreducible 0.01 ($76\times$ gap)
`C16`	M4b Stack $S = 9$	25 nm cristae, $C_S = 25, \delta = \beta = 5 \times 10^{-3}$	24 calibrations; reducible LB $3/4 = 0.75$ vs. irreducible 10^{-3} ($750\times$ gap)

Table 3: Four-test experimental falsification matrix separating H_0 (artifact), H_1 (Regime I passive polariton), and H_2 (Regime II active coherence).

Protocol	H_0 (Artifact)	H_1 ($C_\Delta = 0$)	H_2 ($C_\Delta > 0$)
D_2O FTIR	No 106.6 peak	MP^+ 106.6 ± 0.5	MP^+ 106.6 ± 0.5
CD_2 lipid	Unshifted 71	$\nu_- \to 56$–58	$\nu_- \to 56$–58
2D-IR/$\Delta\Psi_m$	No echo	Pure T_1/inhom.	$T_2^* \geq 0.5\,\mu$s
Oligomycin	Unchanged	Persists (intact)	Drops w/ ATP

2026. bioRxiv preprint 10.64898/2026.09.10.750628v1, 15 September 2026 (unrefereed).

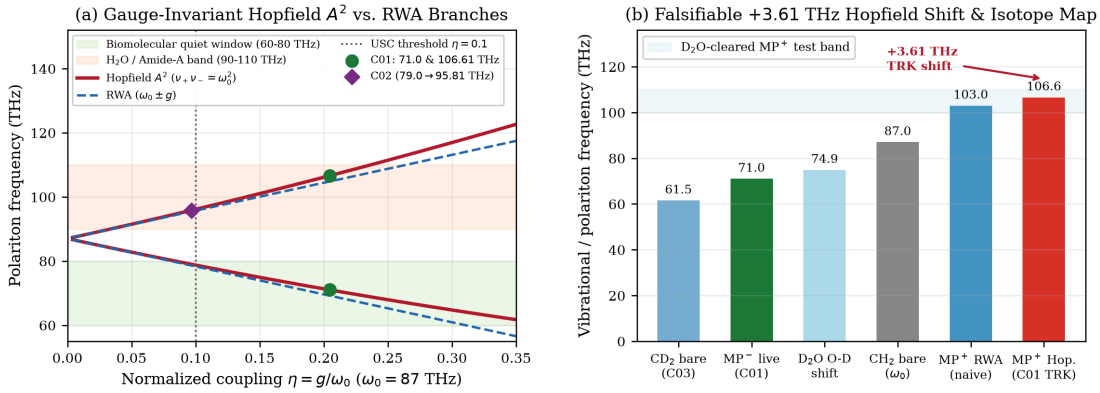

Figure 1: **Gauge-Invariant Hopfield A^2 Spectrum and Isotope Tests.** (a) Exact Hopfield TRK polariton branches ($\nu_+\nu_- = \omega_0^2$) versus naive RWA ($\omega_0 \pm g$) across $\eta = g/\omega_0$, with live certified witnesses `C01` ($\eta = 0.2046$, USC) and `C02`. (b) Direct +3.61 THz blue-shift of MP$^+$ (106.61 vs. 103 THz) exposed when D_2O shifts water absorption to 74.9 THz.

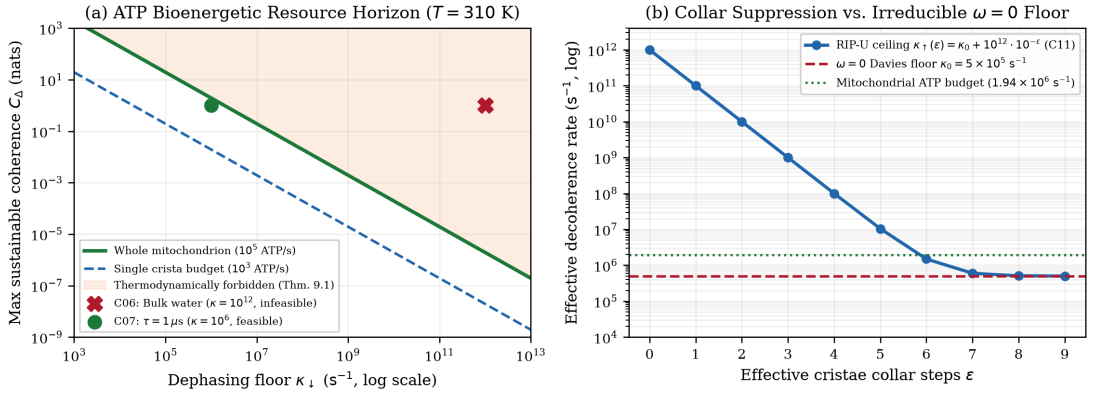

Figure 2: **Bioenergetic ATP Resource Horizon and Cristae Collar Suppression.** (a) Exact log-log feasibility phase diagram from Theorem 9.1 at $T = 310$ K comparing whole-mitochondrion (10^5 ATP/s) and single-crista budgets against bulk-water dephasing (`C06`, infeasible by 5×10^5) and microsecond-suppressed Regime II (`C07`, feasible). (b) RIP-U geometric collar decay hitting an irreducible $\omega = 0$ Davies floor (`C11`).

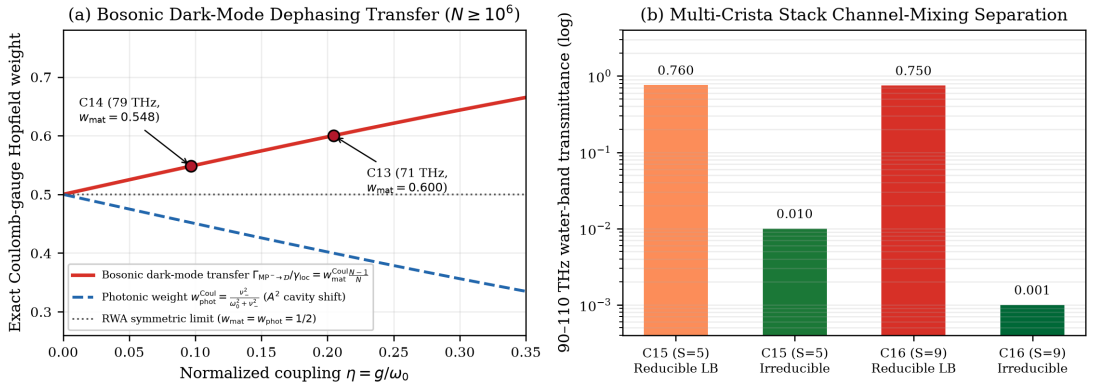

Figure 3: **Bosonic Dark-Mode Dephasing Transfer and Multi-Crista Stack Shielding.** (a) Exact Coulomb-gauge Hopfield lower-polariton matter weight $w_{\mathrm{mat}}^{\mathrm{Coul}} = \omega_0^2/(\omega_0^2 + \nu_-^2) > 1/2$ and dark-mode dephasing transfer $\Gamma_{\mathrm{MP}^- \to \mathcal{D}}/\gamma_{\mathrm{loc}} = w_{\mathrm{mat}}^{\mathrm{Coul}} \frac{N-1}{N}$ vs. η, with certified witnesses `C13` (71 THz, 60.0%) and `C14` (79 THz, 54.8%). (b) Live Mode 4b water-band transmittance separation between factorized single-bilayer filters and irreducible coupled S-lamella cristae stacks (`C15`, `C16`).